2020 8th IEEE International Conference on Biomedical
Robotics and Biomechatronics (BioRob)
New York, USA. Nov 29 - Dec 1, 2020

A Controllable Biomimetic SMA-actuated Robotic Arm

Alireza Golgouneh
Department of Electrical Engineering,
University of Minnesota, Minneapolis,
Minnesota, USA
golgo002@umn.edu

Brad Holschuh
Wearable Technology Lab,
University of Minnesota, Minneapolis,
Minnesota, USA
bth@umn.edu

Lucy Dunne
Wearable Technology Lab,
University of Minnesota, Minneapolis,
Minnesota, USA
ldunne@umn.edu

Abstract— **In this paper, we present a biomimetic 2-DOF SMA-actuated robotic arm that can be controlled by a wearable sleeve in real-time. The designed lightweight robotic arm is intended to be an alternative to the existing heavy and bulky systems, used in different areas such as rehabilitation, haptics and, surgical robotics, etc. which are actuated by the regular hydraulic/pneumatic pistons and brushed/brushless motors. The robotic arm weighs 59g with a wide controllable range of motion (119˚ and 123˚ for the 1st and the 2nd joints, respectively). To enable closed-loop control of the joint angular positions, a PID controller was implemented, and its performance was evaluated. Then, the robot payload was evaluated by finding the maximum torque for each joint. The comparison between the existing commercial DC motors and the designed SMA-actuated rotary joints shows that the performance of the designed SMA-actuated rotary joints are acceptable as they outperform well-known commercial motor-based rotary joints in terms of power consumption, nominal voltage, nominal torque, and mass. Next, an End Effector displacement analysis was conducted to assess the robot positioning. Finally, the entire designed teleoperation system comprising the robotic arm and the wearable measurement sleeve was assessed by performing 20 flexion-extension trials. An average RMSE of 13.1mm was achieved for EE displacement.**

Keywords—Shape Memory Alloy, Biomimetic, Teleoperation, Wearable Technology, Soft robotics

I. INTRODUCTION

Biomimetic robotics is a field of robotics that is concerned with designing and controlling robots that imitate the structure and movement characteristics of animals and humans [1]. Given the flexible and efficient operations and movement characteristics of natural organisms, biomimetic robotics has stimulated the interest of engineers and researchers to look into various applications, such as underwater exploration, biology, surgery, rehabilitation, etc. One of the major subclasses of biomimetic robotics is telerobotics, which is aimed at designing robotic teleoperation systems in which a robot is remotely controlled by a human. The applications of such systems are usually in the fields where tasks should be carried out safely, remotely, and accurately. The Da Vinci robotic system is one of the surgical applications of telerobotics, and is used to perform laparoscopic procedures [2]. Similar to other robotic systems, three factors play essential roles in the success of a telerobotic system: (1) actuation, (2) sensing, and (3) control. Traditionally, hard actuators (such as electromagnetic technologies) have been used as actuators. Although these actuators are able to provide enough power, they are typically heavy and bulky which limits their applications for performing specific tasks, where size and flexibility of actuators matter. In these cases, soft actuators are viable choices which are softer, smaller, and lighter compared to the hard ones. These actuators include but are not limited to Electroactive Polymers and Shape Memory Alloy (SMA) [3]. In addition to actuation, sensing and control are also essential in designing a telerobotics system. In a biomimetic master-slave system, master side sensors are mainly responsible for sensing of human body status to generate a trajectory to be followed by a slave (control signal). On the other hand, slave side sensors determine the state of the system and provide feedback to the control system. Similar to actuators, sensors could be soft or hard and range from force [4], strain [5], and position [6] to physiological sensors [7], [8]. In [9] Li et al. designed a biomimetic system in which the commercial Kinova Jaco robotic arm (6-DOF) is controlled via a glove (6-DOF). The goal of this study was to build an intuitive mapping between the Jaco arm (6-DOF) and the human arm (6-DOF) to grasp objects. Inertial measurement units (IMUs) and force sensors were adopted to provide feedback for the system. Bimbo et al. presented a robotic teleoperation system in which the end effector of the robot was mounted on a 6-DOF robotic arm and wearable vibrotactile armbands and a Leap Motion sensor were used for detection of a posture and position of the hand [10]. In another study Hassan et al. controlled a 5-DoF Aideepen ROT3U robotic arm in real-time based on the users' surface Electromyography (sEMG) signal [11]. One of the problems of the previously proposed systems is that they are based on commercial serial link motor-based robots. These manipulators are relatively heavy and have low payload-to-weight-ratio [12]. Hence, despite the advances in biomimetic teleoperation robotics, the development of lightweight and high payload-to-weight-ratio systems still has room for improvement to become practical in real-life applications.

Therefore, in this study, we will present a novel lightweight biomimetic teleoperation robotic system which is able to mimic users' shoulder and elbow flexion-extension. In

comparison with previous works, our system has improvements in terms of the robot structure, actuation mechanism, control algorithm, and tracking strategies.

II. System Overview

As shown in Figure 1, on the master side of our teleoperation system, two IMUs are placed on upper arm and forearm to capture users' shoulder and elbow flexion-extension. These reference data are transferred through an Arduino microcontroller to the slave-side controller. On the slave side, the robotic arm is actuated by two SMA springs and two IMUs provide feedback to the controller. The controller is responsible for controlling SMA spring actuation by adjusting the electrical power such that the robot mimics the reference trajectory.

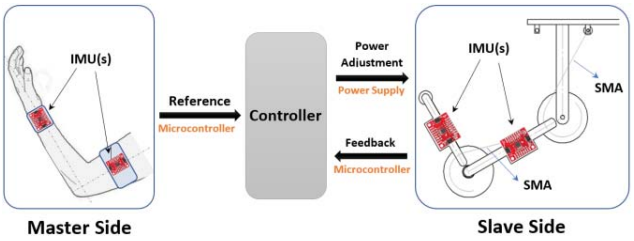

Figure 1. Proposed teleoperation biomimetic system schematic

III. Experimental Setup

A. Actuators

SMA actuators are used to move the designed robotic arm. SMAs belong to a class of specific materials capable of memorizing or retaining a trained shape after exposure to certain thermomechanical or magnetic stimulus, referred to as the shape memory effect (SME). SMAs can be made out of different types of alloys such as Gold-Cadmium and Copper-Zinc-Aluminium, and Nickel-Titanium which is known as Nitinol (or NiTi) and is more common than the other types. The SME effect of the SMA takes place due to a transformation of the crystalline structure between Martensite and Austenite phases. At lower temperatures, the material is in its Martensite phase where it is relatively soft and deformable. When the SMA is heated, the transformation from Martensite to Austenite phases occurs, leading to a decrease in a SMA wire length and bulk change in actuator shape. The reversible transition between these two phases results in actuation and force generation. In addition to the SME characteristic of these materials, pseudo-elasticity and bio-compatibility are the other salient features of these materials which have made them ideal for a wide variety of applications in different areas, such as biomedical engineering, aerospace engineering, and robotics [13], [14]. Given that the maximum recoverable actuation stroke of straight SMA wire is only ~5% of its length [14], here we adopted the method used in [15] to shape the SMA wires into springs to achieve a significantly greater (>50%) recoverable actuation stroke.

B. Robot Structure Design

The structure of our robot is designed based on previous work presented in [16] and [17]. Guo et al. designed and controlled a 1-DOF robot, actuated by a SMA wire. Their robot was composed of two 370mm antagonistic SMA wires and a mechanical joint coupled with a torsion spring (compliant differential configuration). They achieved a range of motion of 30° with this configuration [17]. In another study, the same range of motion was achieved for a 1-DOF manipulator with a 370mm SMA actuator and 100mm link length [16]. Compared to these studies, here we propose a design for a 2-DOF robot manipulator which has shorter actuators but greater range of motion. It should be noted that, as will be discussed in section IV, adding an additional DOF and replacing the SMA wires with SMA springs adds complexity and uncertainties to the system which makes controlling the robot more challenging due to the inherent nonlinear behavior of this material [18].

In Figure 2, a Computer Aided Design (CAD) model of our 2-DOF robotic arm, together with the location of the IMUs on links are shown. Also, the fabricated robotic arm, as well as the two IMUs responsible for measuring the angular position of each joint and providing feedback for the closed-loop controller, can be seen in Figure 12. This robotic arm has three links (94mm, 112mm, and 87mm). The two SMA spring actuators with lengths of 50mm and 40mm (at their Austenite Finish (A_f) temperature) have been attached to one end of two 17mm radius rotary joints. The structure of the robot (including links, joints, and base parts) was manufactured using a LulzBot TAZ 5 3D printer and was constructed using polylactic acid (PLA). In order to ease the joints' rotations and withstand an axial load (thrust), a 604ZZ Miniature Single Row Deep Groove Ball Bearing was mounted on a rotation shaft to fit into the joint housing. The specifications of the robot components are mentioned below.

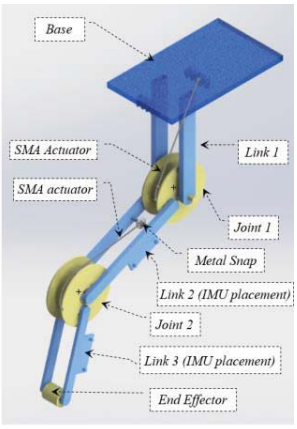

Part Name	Mass (g)	Length (mm)
Base + Link1	64	94
Joint 1	11	-
Link 2 (left)	9	112
Link 2 (right)	9	112
Joint 2	11	-
Link 3 (left)	7	87
Link 3 (right)	7	87
End Effector	5	-

Figure 2. Proposed 2-DOF SMA spring actuated robotic arm CAD and its component properties

C. Wearable Sleeve Design

The designed wearable system consists of a sleeve made out of flexible and stretchable material, and an adjustable back support posture brace for housing the microcontroller and two IMUs. To prevent IMUs from moving on the upper arm and forearm, the sleeve was made tight enough to ensure that the IMUs were aligned and placed on a same plane when the user's hand was straight. This wearable sleeve is shown in Figure 3.

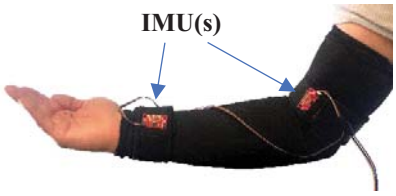

Figure 3. Wearable Measurement Sleeve

D. Hardware and Equipment

a) Data Collection System

Four BNO080 IMU modules were used to measure the rotation. Two of these were placed on the robotic arm as feedback sensors in a closed-loop position control system and the other two were sewn on the wearable sleeve to be placed on the upper arm and forearm sections to find the desired input signals to the closed-loop control system. The BNO080 IMU features a 32-bit ARM Cortex M0+ to produce accurate rotation vectors. Two Arduino UNOs with mounted SparkFun Qwiic Shields on top were used to collect the IMUs data. The sampling frequency of the data collection system was set to 80Hz.

b) Power Control System

As stated earlier in section V, to control the activation of the actuators, the temperature of the SMA wires must be controlled which can be done by controlling the supplied electrical power, known as the resistive heating approach. To do so, a KEITHLEY 2230G-30-6 programmable power supply was used to control the current through the National Instruments® VISA-USB interface.

c) Static Force Analysis System

In order to analyze the mechanical/actuation behavior of the SMAs (which will be detailed in section IV) an Instron 360 Series Universal Testing System was used.

IV. Actuator Force-Voltage Analysis

The first test was conducted to characterize the behavior of the actuators under a fixed extensional strain condition at 145mm. In this test, an actuator was held at a fixed extensional strain (145mm) and exposed to increasing currents from 0 to 1500mA at 50 mA increments, 25 seconds per step. According to Figure 4, there was no significant increase in the force at powers < 0.72W (= 0.3A), at which point the temperature was not yet high enough for the actuators to respond. For power values greater than 0.72W (=0.3A) the force progressively increases. At 10.2W the force profile reaches a maximum, meaning that the force does not change by increasing the power. This is a result of overheating the actuator to the point that the SMA memory state begins to reset due to excessive Joule heating. This point is critical for designing the robot joints, as the SMA actuator is not able to produce force due to SME loss. Therefore, in order to avoid overheating and consequently activation force loss, the maximum power of 2.87W (4.78V, 0.6A) was chosen for the activation of the actuators. The Force-Power profiles for the actuators are shown in Figure 5.

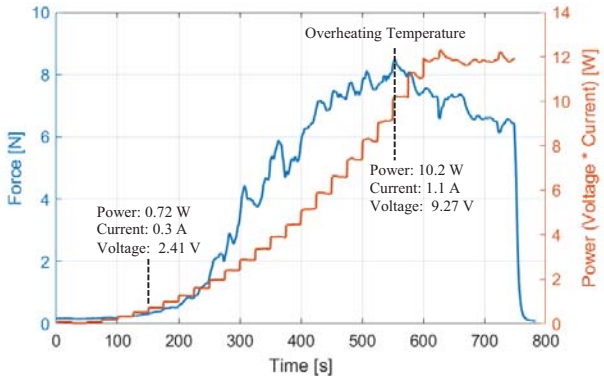

Figure 4. Actuator Force-Power (Voltage×Current) relationship for a fixed strain (145mm)

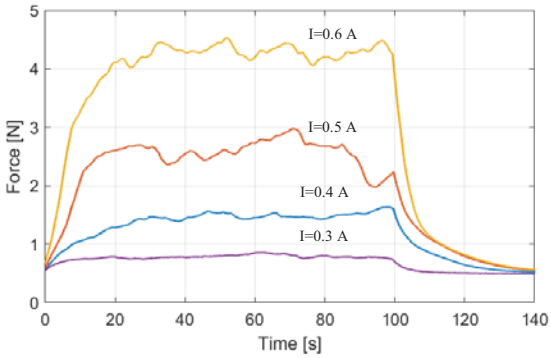

Figure 5. Force profiles of the actuator, activated by 0.3A, 0.4A, 0.5A, and 0.6A currents.

V. Closed-loop Position Control

To regulate the position of the robot arm's end-effector, a PID controller was adopted. To do so, the angular position of each joint is controlled separately. The block diagram of the implemented controller is depicted in Figure 6. As stated earlier, in this system, the current was chosen as a control variable (u) and u_{sat} was set to 0.6A.

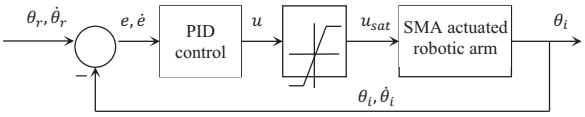

Figure 6. PID controller block diagram

Having considered rise time, overshoot, settling time, steady-state error, and stability of the system, the PID gains for the two joint controllers were adjusted heuristically. The effects of varying PID parameters (K_p, K_i, K_d) on the angular positions of the two joints are shown in Figure 7 and Figure 8. Here, it is important to emphasize that due to the highly nonlinear and unpredictable behavior of the SMA actuators under different loading and heating conditions, the response stability is critical and overweight the other factors. Our experimental results showed that the PD controller performs relatively better than the other types of PID control (such as P, PI or PID) in terms of the rise time, overshoot, settling time, and steady-state error. Hence, the PD gains of independent controllers for each joint were tuned

heuristically and set to $K_p = 0.2, K_i = 0, K_d = 0.1$ for the 1st and $K_p = 0.1, K_i = 0$, and $K_d = 0.1$ for the 2nd joints.

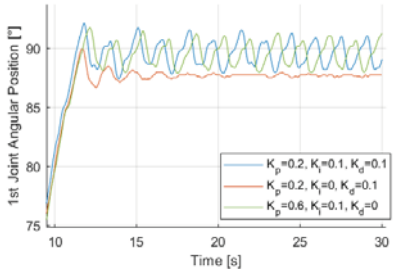

Figure 7. Adjusting PID controller gains for 1st robot joint with respect to its angular position (Desired setpoint: 90°)

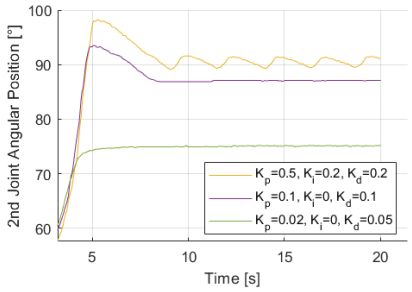

Figure 8. Adjusting PID controller gains for 2nd robot joint with respect to its angular position (Desired setpoint: 90°)

VI. Teleoperation System Performance Analysis

In this section, we assess the performance of the designed wearable robotic system. To this end, we first examine the robot joint's torque production. Then we evaluate the robotic arm motion, using the resultant displacement of the robot End Effector. Next, we evaluate the functionality of the entire system as a biomimetic SMA-actuated robotic arm.

A. Robot Joint Torque Analysis

To analyze the producible torque by each joint, different weights were attached to the end effector, and the joint torque was calculated by $\tau = F.r.\sin(\alpha)$ where F is force, r is the length of the arm, and α is the angle between the force vector and the moment arm. Thus, in order to measure the maximum producible torque by each joint, they were set to lift various masses (from 7 to 71 grams) to 90 degrees (i.e., perpendicular to gravitational acceleration). The experiment results are presented in Figure 9 and Figure 10. As shown in these figures, the robot's first joint is able to lift up the masses up to 56g while this figure for the second joint is 62g. It is worth mentioning that frictional properties and geometry of the surfaces in contact with each other, position and alignment of the shafts and bearings, setup wiring constraints, etc. are the unwanted factors that affect the amount of torque each joint can generate. Having considered these undesirable factors and the length of the links (see Figure 2) the minimum-maximum torque values for the first (τ_1) and second joint (τ_2) are computed as:

$$\tau_1 = 0.112 \times 0.056 \times 9.8 = 0.061\ N.m = 61mNm \quad (1)$$

$$\tau_2 = 0.087 \times 0.062 \times 9.8 = 0.052\ N.m = 52mNm \quad (2)$$

To better understand these torque values, the specifications of the four commercial Maxon Brushed DC Motors having the same range of nominal torque, have been listed in Table 1. In this table, input electrical power or electrical power consumption is computed as the denotes the product of nominal current and voltage. Also, the weight of the link 2 (left and right) together with the joint weight (mentioned in Figure 2) were considered as the SMA-based joint mass. The performance of the designed SMA-actuated rotary joint is acceptable, as it outperforms motor based rotary joints in terms of power consumption, nominal voltage, nominal torque, and mass. Here, we should take into consideration that rotation of the SMA-based joints is very slow (~10 RPM) compared to these DC motors and they are not designed to conduct a continuous rotation.

Table 1. A comparison between the fabricated SMA-actuated rotary joint and four commercial Maxon Brushed DC Motors

Part NO.	Input electrical power (W)	Nominal voltage (V)	Nominal current (mA)	Nominal torque (mNm)	Mass (g)
108828	8.01	15	534	6.93	54
268193	48	12	4000	51.7	260
302002	13.5	9	1500	11.1	130
448593	16.2	6	2700	53	260
SMA-based joint	**2.87**	**4.78**	**600**	**61**	**29**

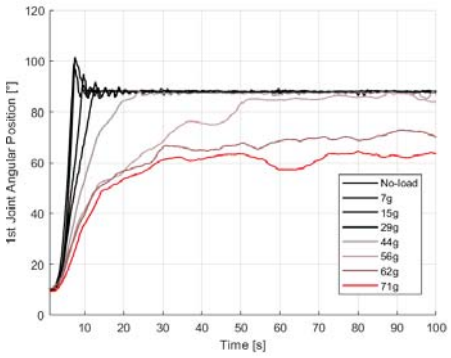

Figure 9. Performance of the robot 1st joint under various loading conditions

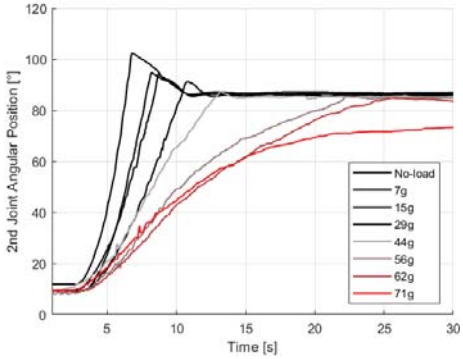

Figure 10. Performance of the robot 2nd joint under various loading conditions

B. End Effector Displacement Analysis

In this section, we analyze the positioning of the Robot End Effector (EE). As mentioned in Table 2, the robot was tested in four different configurations. For each configuration, the Root Mean Square Error (RMSE) for the 1st joint angular position (θ_{a1}), the 2nd joint angular position (θ_{a2}), and EE were calculated under two loading conditions. According to

this table, the range of RMSEs for θ_{a1} in the loaded condition are relatively higher than those of θ_{a1} in the no-load condition, while these figures are opposite for θ_{a1}. This is due to the fact that in order to minimize the power consumption, the robot is designed such that the robot EE weight returns the robot downward. Hence, adding an external mass increases the inertia applied on the second joint and helps it go back to its initial position after overshooting (See Figure 10). The average calculated RMSE for EE displacement in all the configurations under no-load and loading conditions, are similar at 11.2 (mm). It should be mentioned that as stated earlier, since the behavior of the SMA actuators is highly nonlinear even at fixed strains (see Figure 5), the PD controller gains were tuned such that the robot had better stability and settling time. However, as can be seen in Figure 7 and Figure 8, there are steady-state errors of 2.7° and 2.1° for the 1st and the 2nd joints which are inevitable with the existing robot configuration, leading to the RMSEs listed in Table 2. The effect of the steady-state error can be seen in Figure 11 as well.

Table 2. The RMSEs between the angular (°) and actual (mm) position of the robot joints (θ_{a1}, θ_{a2}) and End Effector (EE)

	No-load Condition			Loaded Condition (7g)		
Configuration	θ_{a1} RMSE (°)	θ_{a2} RMSE (°)	EE RMSE (mm)	θ_{a1} RMSE (°)	θ_{a2} RMSE (°)	EE RMSE (mm)
$\theta_{a1}=30°$ $\theta_{a2}=30°$	1.8	1.1	1.7	2.0	1.9	6.8
$\theta_{a1}=45°$ $\theta_{a2}=45°$	2.2	4.1	10.6	2.2	1.1	6.0
$\theta_{a1}=90°$ $\theta_{a2}=90°$	2.5	15.8	19.0	4.3	1.7	10.6
$\theta_{a1}=120°$ $\theta_{a2}=120°$	8.3	18.6	13.1	9.0	2.6	21.6
Average	3.7	9.9	11.1	4.3	1.8	11.2

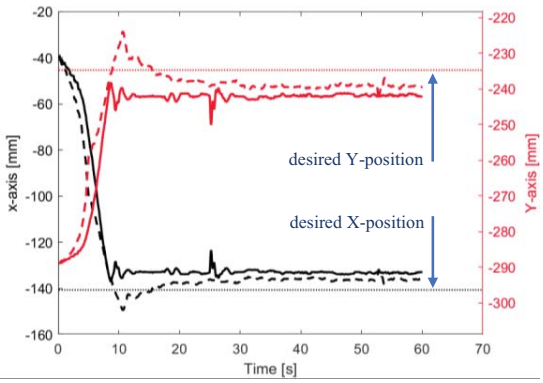

Figure 11. The effect of the steady-state error on the End Effector position plotted for $\theta_{a1}=45°$, and $\theta_{a2}=45°$ configuration (dashed line: loaded by 7g mass, solid line: no-load)

C. *Wearable System Performance Analysis*

Twenty 48- to 120-second flexion-extension trials were conducted to analyze the entire biomimetic teleoperation system. In each trial, a subject conducted a random shoulder-elbow flexion-extension while the robotic arm followed these movements in real-time. Figure 12 shows photographs captured while a subject was performing the elbow flexion. Prior to conducting the trials, all IMUs were calibrated [19]; then, their position and alignment were adjusted. On the slave side, the robot links were already designed with the pair of IMUs aligned and placed on the same plane. On the master side, while the user's arm was straight, the two IMUs placed on the upper arm and forearm were aligned such that their outputs (quaternions) matched. Next, the calculated elbow and shoulder angles were validated using a Vicon Motion Capture System. In order to reduce IMU noise and artifacts, an online Moving Average filter with a length of 40 was adopted to smooth both the reference trajectory (master side) and feedback (slave side) signals before inputting to the controller. Figure 13 shows the human arm (reference) and the robot EE (follower) smoothed trajectories. The average RMSE for all the trials was computed as 13.1mm.

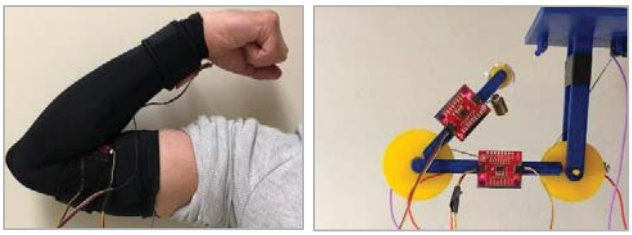

Figure 12. Real-time implementation of the designed wearable system

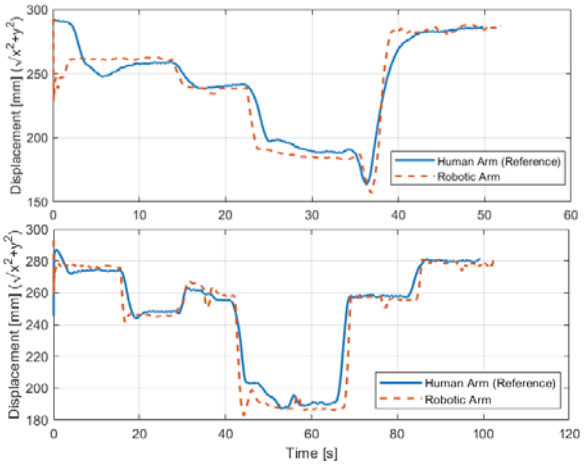

Figure 13. Human arm (reference) and the follower robot EE trajectories

VII. Conclusion, Limitations and Future Works

In this paper, we have presented a novel biomimetic system in which a robotic arm mimics an operator's arm movement. In this system a 2-DOF SMA-actuated robotic arm is controlled by a wearable measurement sleeve in real-time. The designed lightweight robotic arm is intended to be an alternative to the existing heavy and bulky systems used in different areas (such as rehabilitation [6], [20], haptics, and surgical robotics for instance) which are actuated by the regular hydraulic/pneumatic pistons and brushed/brushless motors. The structure of the robotic arm discussed here weighs 59g and has a wide controllable range of motion of 119° for the 1st joint and 123° for the 2nd joint. A PD controller was adopted to provide closed-loop control of the joint angular positions. Due to the nonlinear and unpredictable behavior of the SMA actuators, the PD controller gains were regulated to better stabilize the system. However, the

inevitable steady-state errors of 2.7˚ and 2.1˚ for the 1st and the 2nd joints lead to average RMSE of 11.2mm for EE displacement. Finally, the entire teleoperation system comprised of the robotic arm and the wearable measurement sleeve was assessed by performing 20 trials of shoulder and elbow flexion-extension and calculating the average RMSE (13.1mm) for all the trials. In comparison with servo-based robotic arms (with angular position accuracy of less than 0.1˚), the error rate of our SMA-based robotic arm is relatively higher. One of the reasons for this is that unlike the servo motors, our robot lacks a gearbox or an anti-backlash mechanism to maintain the generated torque and reduce the actuation oscillations which lead to error in joint movements. Therefore, using latching mechanisms in the future could possibly help to reduce the error rates [21]. Furthermore, one of the biggest challenges of working with SMAs is that they exhibit nonlinear unpredictable time-variant behavior even under constant loading and temperature-controlled conditions. This problem is exacerbated while working with SMA springs (instead of wire), as we saw in section IV. Therefore, other controllers such as sliding mode [22], [23], optimal [24], [25], robust [26], ELM [27], etc. could be implemented on this biomimetic teleoperation system to achieve better performance and lower error rate. Also, to achieve higher forces and faster actuation, SMA springs could be activated by higher electrical power, up to 10.2W (=1.1A). However, increasing the input power may increase the risk of overheating and subsequently activation force loss. Moreover, using multiple actuators in different configurations could improve the robot performance, but it would affect the power consumption and system cooling requirements.

VIII. Acknowledgement

This work was supported by the US National Science Foundation under grant #1722738.

IX. References

[1] L. D. Paulson, "Biomimetic robots," *Computer (Long. Beach. Calif).*, vol. 37, no. 9, pp. 48–53, 2004.

[2] J. Bodner *et al.*, "The da Vinci robotic system for general surgical applications: A critical interim appraisal," *Swiss Med. Wkly.*, 2005.

[3] C. Laschi, B. Mazzolai, and M. Cianchetti, "Soft robotics: Technologies and systems pushing the boundaries of robot abilities," *Science Robotics*. 2016.

[4] M. I. Tiwana, S. J. Redmond, and N. H. Lovell, "A review of tactile sensing technologies with applications in biomedical engineering," *Sensors and Actuators, A: Physical*. 2012.

[5] A. Golgouneh, M. Tahmidul Islam Molla, and L. E. Dunne, "A comparative feasibility analysis for sensing swelling with textile-based soft strain sensors," in *Proceedings - International Symposium on Wearable Computers, ISWC*, 2019.

[6] A. Golgouneh, A. Bamshad, B. Tarvirdizadeh, and F. Tajdari, "Design of a new, light and portable mechanism for knee CPM machine with a user-friendly interface," in *Artificial Intelligence and Robotics (IRANOPEN), 2016*, 2016, pp. 103–108.

[7] A. Golgouneh and B. Tarvirdizadeh, "Fabrication of a portable device for stress monitoring using wearable sensors and soft computing algorithms," *Neural Comput. Appl.*, Jun. 2019.

[8] B. Tarvirdizadeh, A. Golgouneh, F. Tajdari, and E. Khodabakhshi, "A novel online method for identifying motion artifact and photoplethysmography signal reconstruction using artificial neural networks and adaptive neuro-fuzzy inference system," *Neural Comput. Appl.*, pp. 1–18, 2018.

[9] S. Li, R. Rameshwar, A. M. Votta, and C. D. Onal, "Intuitive Control of a Robotic Arm and Hand System with Pneumatic Haptic Feedback," *IEEE Robot. Autom. Lett.*, 2019.

[10] J. Bimbo, C. Pacchierotti, M. Aggravi, N. Tsagarakis, and D. Prattichizzo, "Teleoperation in cluttered environments using wearable haptic feedback," in *IEEE International Conference on Intelligent Robots and Systems*, 2017.

[11] H. F. Hassan, S. J. Abou-Loukh, and I. K. Ibraheem, "Teleoperated robotic arm movement using electromyography signal with wearable Myo armband," *J. King Saud Univ. - Eng. Sci.*, 2019.

[12] T. Yano, M. Kaneko, and M. Sonoda, "Development of a synchronous motor with three degrees of freedom," in *Theory and Practice of Robots and Manipulators*, Springer, 1995, pp. 275–280.

[13] S. Kazeminasab, A. Hadi, K. Alipour, and M. Elahinia, "Force and motion control of a tendon-driven hand exoskeleton actuated by shape memory alloys," *Ind. Rob.*, 2018.

[14] A. Hadi, K. Alipour, S. Kazeminasab, and M. Elahinia, "ASR glove: A wearable glove for hand assistance and rehabilitation using shape memory alloys," *J. Intell. Mater. Syst. Struct.*, 2018.

[15] B. Holschuh and D. Newman, "Low spring index, large displacement shape memory alloy (sma) coil actuators for use in macro-and micro-systems," in *Reliability, Packaging, Testing, and Characterization of MOEMS/MEMS, Nanodevices, and Nanomaterials XIII*, 2014, vol. 8975, p. 897505.

[16] S. Quintanar-Guzmán, S. Kannan, A. Aguilera-González, M. A. Olivares-Mendez, and H. Voos, "Operational space control of a lightweight robotic arm actuated by shape memory alloy wires: A comparative study," *J. Intell. Mater. Syst. Struct.*, 2019.

[17] Z. Guo, Y. Pan, L. B. Wee, and H. Yu, "Design and control of a novel compliant differential shape memory alloy actuator," *Sensors Actuators, A Phys.*, 2015.

[18] M. H. Elahinia and H. Ashrafiuon, "Nonlinear control of a shape memory alloy actuated manipulator," *J. Vib. Acoust. Trans. ASME*, 2002.

[19] sparkfun, "BNO080 Sensor Calibration Procedure." [Online]. Available: https://cdn.sparkfun.com/assets/c/6/f/4/9/Sensor-Calibration-Procedure-v1.1.pdf.

[20] P. Nomanfar, A. Tekin, S. Bogosyan, and P. Sendur, "Design and Kinematics of 4- DoF Multi-Purpose Wearable Mechanical Arm (MUWA) Support for Enhanced Operation Stability," in *Proceedings - 2019 IEEE International Conference on Mechatronics, ICM 2019*, 2019.

[21] M. E. Clarke, L. E. Dunne, and B. T. Holschuh, "Self-Adjusting wearables: Variable control through a shape-memory latching mechanism," in *UbiComp 2016 Adjunct - Proceedings of the 2016 ACM International Joint Conference on Pervasive and Ubiquitous Computing*, 2016.

[22] A. Aalipour, H. Kebriaei, and M. Ramezani, "Nonlinear Robust Traffic Flow Control in Urban Networks," *IFAC-PapersOnLine*, 2017.

[23] F. Tajdari, M. Kabganian, E. Khodabakhshi, and A. Golgouneh, "Design, implementation and control of a two-link fully-Actuated robot capable of online identification of unknown dynamical parameters using adaptive sliding mode controller," in *7th Conference on Artificial Intelligence and Robotics, IRANOPEN 2017*, 2017.

[24] F. Tajdari, E. Khodabakhshi, M. Kabganian, and A. Golgouneh, "Switching controller design to swing-up a two-link underactuated robot," in *2017 IEEE 4th International Conference on Knowledge-Based Engineering and Innovation (KBEI)*, 2017, pp. 595–599.

[25] A. Aalipour, H. Kebriaei, and M. Ramezani, "Analytical Optimal Solution of Perimeter Traffic Flow Control Based on MFD Dynamics: A Pontryagin's Maximum Principle Approach," *IEEE Trans. Intell. Transp. Syst.*, 2019.

[26] F. Tajdari, M. Kabganian, N. F. Rad, and E. Khodabakhshi, "Robust control of a 3-DOF parallel cable robot using an adaptive neuro-fuzzy inference system," in *2017 Artificial Intelligence and Robotics (IRANOPEN)*, 2017, pp. 97–101.

[27] A. Kalhor, N. Hojjatzadeh, and A. Golgouneh, "Potentials of Evolving Linear Models in Tracking Control Design for Nonlinear Variable Structure Systems," *Amirkabir Int. J. Model. Identification, Simul. Control*, vol. 48, no. 2, pp. 75–92, 2016.